CrossMark

JfM PAPERS

Viscoelastic levitation

Yunxing Su[1], Alfonso Castillo[2,3], On Shun Pak[4], Lailai Zhu[5] and Roberto Zenit[1,2],†

[1]Center for Fluid Mechanics, School of Engineering, Brown University, Providence, RI 02912, USA

[2]Instituto de Investigaciones en Materiales, Universidad Nacional Autónoma de México, Ciudad de México 04510, México

[3]Departamento de Ingeniería Química, Facultad de Química, Universidad Nacional Autónoma de México, Ciudad de México 04510, México

[4]Department of Mechanical Engineering, Santa Clara University, Santa Clara, CA 95053, USA

[5]Department of Mechanical Engineering, National University of Singapore, 117575, Republic of Singapore

The effects of viscoelasticity have been shown to manifest themselves via symmetry breaking. In this investigation, we show a novel phenomenon that arises from this idea. We observe that when a dense sphere is rotated near a wall (the rotation being aligned with the wall-normal direction and gravity), it levitates to a fixed distance away from the wall. Since the shear is larger in the gap (between the sphere and the wall) than in the open side of the sphere, the shear-induced elastic stresses are thus asymmetric, resulting in a net elastic vertical force that balances the weight of the sphere. We conduct experiments, theoretical models and numerical simulations for rotating spheres of various sizes and densities in a Boger-type fluid. In the small-Deborah-number range, the results are collapsed into a universal trend by considering a dimensionless group of the ratio of elastic to gravitational forces.

Key words: particle/fluid flow, viscoelasticity

1. Introduction

The study of classical Newtonian fluid flows constitutes the foundation of fluid mechanics. Through experiments, theory and numerical solutions, we have gained a vast insight into the nature of flow for a wide range of conditions, from laminar to turbulent. The situation is very different for complex fluids (Larson 1999). In many such cases, the presence

† Email address for correspondence: zenit@brown.edu

of memory and stress anisotropy change substantially the nature of the flow, leading to dramatic differences. For instance, a two-dimensional shear flow gives rise to non-zero normal stresses in a viscoelastic fluid, unlike in a Newtonian fluid. Many of the surprising phenomena seen in the flow of complex fluids, and in viscoelastic fluids in particular, can be understood by an examination of these normal stresses and the normal stress differences (Morozov & Spagnolie 2015).

The general mechanism for the appearance of normal stress can be explained by the following arguments. Polymers are stretched and rotated under the action of the local shear and tend on average to align with the streamlines, while the entropic forces acting to return the molecule to its undisturbed conformation lead to an extra tension in the direction of the flow. Some well-known examples are the Weissenberg effect and die swell in fluid extrusion. In addition to large-scale collective effects, the presence of normal stress differences in flow can be important on smaller scales as well: cells and other soft biological matter may experience extra polymeric stresses that lead to deformation or possibly rupture (Morozov & Spagnolie 2015). Similar to cell migrations in blood vessels, researchers (Halow & Wills 1970; Ho & Leal 1976; d'Avino *et al.* 2010) show that due to the imbalanced normal stresses, in a simple shear flow particles close to the centre plane of the set-up tend to move towards the nearest wall. Many microorganisms swim through fluids that display non-Newtonian characteristics. For example, as spermatozoa make their journey through the female reproductive tract, they encounter several complex fluids, including glycoprotein-based cervical mucus in the cervix (Katz, Mills & Pritchett 1978), mucosal epithelium inside the fallopian tubes, and an actin-based viscoelastic gel outside the ovum (Dunn & Picologlou 1976; Suarez & Pacey 2006). These complex fluids often have dramatic effects on the locomotion of microorganisms. The presence of time-dependent stresses, normal stress differences, and shear-dependent material functions in complex fluids are able to alter fundamentally the physics of locomotion (Purcell 1977; Lauga & Powers 2009).

Propulsive forces can also result from the secondary flows induced by non-Newtonian normal stress differences; a theoretical investigation that further exemplifies these complexities is that by Normand & Lauga (2008). They considered a biologically inspired geometric example of a semi-infinite flapper performing reciprocal sinusoidal motion in a viscoelastic Oldroyd-B fluid in the absence of inertia. They showed explicitly that the reciprocal motion generates a net force on the flapper occurring at second order in the flapping amplitude, and disappearing in the Newtonian limit as dictated by the scallop theorem, but there was no time-average flow accompanying the net force generation. Also, Pak, Normand & Lauga (2010) reported on the discovery of a net fluid flow produced by the reciprocal flapping motion in an Oldroyd-B fluid. The net flow transport was seen to occur at fourth order in the flapping amplitude, and was due to normal stress differences. The dependence of the pumping performance on the actuation and material parameters was characterized analytically, and the optimal pumping rate was determined numerically. Through this example, they therefore demonstrated explicitly the breakdown of the scallop theorem in complex fluids in the context of fluid pumping, and suggested the possibility of exploiting intrinsic viscoelastic properties of the medium for fluid transport on small scales.

The investigation by Pak *et al.* (2012) is very relevant for the present paper. They reported that a two-sphere rotating dimer (snowman geometry) was capable of self-propelling in a complex fluid if the two spheres were of different sizes. The motion results from the asymmetry and the presence of normal stress differences under rotational actuation. Physically, the direction in which such an object moves can
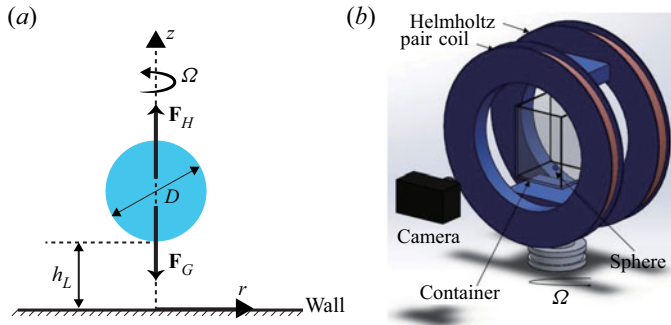
Figure 1. (*a*) Schematic of a sphere of diameter D rotating above a plane wall at a constant rotational rate Ω about the z-axis. When the levitating hydrodynamic force $\boldsymbol{F}_H$ on the sphere balances its own gravitational force $\boldsymbol{F}_G$, the bottom of the sphere stays at a levitation height $h = h_L$ above the wall. (*b*) The experimental set-up consists of a spherical particle inserted with permanent magnets placed inside a container of test fluid under a Helmholtz pair coil.

be understood by means of the hoop stresses generated along curved streamlines. A secondary, purely elastic flow is created by each rotating sphere, contracting in along the equator of each sphere and flowing out of the poles. Because the spheres are unequal in size, hydrodynamic interactions due to this secondary flow are unbalanced, leading to propulsion in the direction of the smallest sphere. Puente-Velázquez *et al.* (2019) verified these findings experimentally using a magnetic snowman immersed in a Boger-type fluid. Recently, Binagia & Shaqfeh (2021) studied a mathematical model of two linked spheres rotating in opposite directions, which is a force- and torque-free swimmer. For this configuration, the swimming direction was found to be towards the larger sphere instead of the smaller one, which is opposite to what was found previously (Pak *et al.* 2012; Puente-Velázquez *et al.* 2019). In addition, the asymmetry between the head and tail of a helical swimmer was reported to be responsible for the swimming speed enhancement of helical swimmers in viscoelastic fluids (Angeles *et al.* 2021).

Other studies have also shown that a wall can break the symmetry of flow leading to the propulsion of a dimer with equal spheres (Keim, Garcia & Arratia 2012) and a three-sphere microswimmer (Daddi-Moussa-Ider *et al.* 2018). Other related investigations include the effect of the hydrodynamic interactions between two neighbouring microswimmers near a wall (Li & Ardekani 2014), given that boundaries have been shown to induce order in collective flows of bacterial suspensions (Woodhouse & Goldstein 2012; Wioland *et al.* 2013, 2016), leading to potential applications in autonomous microfluidic systems (Woodhouse & Dunkel 2017).

In this work we introduce a novel phenomenon that arises from the effect of viscoelasticity via symmetry breaking. We observed experimentally that when a dense sphere is rotated near a wall being immersed in a viscoelastic fluid, it levitates to a fixed distance from the wall. We refer to this phenomena as 'viscoelastic levitation'. The arrangement considered here is shown schematically in figure 1(*a*). Spheres of various sizes and densities were tested in a Boger-type fluid (Boger 1977; James 2009) in experiments. We also develop a theoretical model that captures the dependence of the levitation height on the experimental parameters. A dimensionless group is identified to collapse the levitation results from experiments.

943 A23-3

Sphere	Diameter (mm)	Mass (mg)	Density (kg m^{-3})
D1 (green squares)	7.99	585	2190.37
D2 (black circles)	8.72	760	2189.10
D3 (navy diamonds)	8.81	819	2287.48
D4 (red downward-pointing triangles)	9.57	1005	2189.94
D5 (cyan upward-pointing triangles)	13.0	1870	1626
D6 (magenta circles)	16.0	3170	1478

Table 1. Physical properties of the spheres used in this investigation.

Fluid	ρ (kg m^{-3})	η_0 (Pa s)	Power-law index n	λ (s)
Newtonian fluid (NF)	1510	0.840	1.00	0.00
Boger fluid I (BF-I)	1508	0.844	0.96	0.51
Boger fluid II (BF-II)	1347	2.9	0.98	0.34

Table 2. Physical properties of the fluids used in this investigation.

2. Experimental set-up and test fluids

2.1. *Experimental set-up*

All experiments in this paper were conducted using the magnetic set-up developed by Godínez, Chávez & Zenit (2012), shown in figure 1(*b*). The device is capable of producing a magnetic field of 6 mT of uniform strength; the field is rotated mechanically. The spheres were placed inside a rectangular tank (160 mm × 100 mm × 100 mm) that fits into the region of uniform magnetic field inside the coils of approximately $100 \times 100 \times 100$ mm^3 in size where the test fluids were contained. The spheres were made out of plastic, inside which several permanent magnets were inserted (Magcraft, models NSN0658). For all the cases, the angular frequency of the rotating coils was below the step-out frequency (Godínez *et al.* 2012); in other words, the sphere rotated at the same rate as the external magnetic field.

Six spheres were tested. Table 1 shows the properties of all spheres. Two spheres (D2 and D3) had approximately the same diameter but different densities; and three spheres (D1, D2 and D4) had approximately the same density but different diameters. Two spheres (D5 and D6) had small densities but larger diameters. The sphere was placed initially at the bottom of the tank at rest, and then driven by the external magnetic field to rotate with the rotating velocity vector normal to the horizontal plane wall (figure 1). A camera was used to record the motion of the sphere rotating in the fluid, and the recorded videos were used in the data analysis to track the vertical position of the sphere.

2.2. *Test fluids*

Two types of fluids were fabricated, tested and used: one is Newtonian reference fluid (NF), and the other is Boger-type fluid (BF) (nearly constant shear viscosity but with viscoelastic properties). Table 2 summarizes the rheological properties of both fluids. To test the effect of changing the viscoelastic relaxation time, two different Boger fluids were prepared (BF-I and BF-II).

The Boger-type fluids were prepared by dissolving polyacrylamide (PAA, molecular weight 5×10^6 g mol^{-1}) in non-ionic water with slow mixing for 24 hours.

Afterwards, the polymeric solution was added to a corn syrup solution with slow mixing over four days. The recipes (mass percentage of glucose, water and PAA) are (84.96 %, 15 %, 0.04 %) and (87.95 %, 12 %, 0.05 %), respectively. After the mixing, the solution was left untouched for 2 weeks to remove the residual bubbles in the fluid before testing. The Newtonian fluid was made by mixing non-ionic water with glucose and adjusting the percentage of water until the fluid showed a viscosity similar to that of the Boger fluid. All the fluids were stored and used in closed containers to avoid free surface crystallization. The rheological properties of the fluids were measured using a shear-rate controlled rheometer (Anton Paar, and ARES-G2, TA Instruments) with a cone-plate geometry. Both steady shear and oscillatory tests were conducted. Note that different batches of corn syrup were used to prepare BF-I and BF-II. In both cases, the fluids had nearly constant viscosity and strong viscoelastic behaviour, but their rheological characterizations were different.

The details of the rheological characterization of the BF-I fluid can be found in Castillo *et al.* (2019), but its salient features are summarized here. The steady shear behaviour of this fluid was found to agree very well with the the Oldroyd-B model (Oldroyd 1950). The measured first normal stress difference, N_1, agreed very closely with

$$N_1 = 2\eta_0(1 - \zeta)\lambda\dot{\gamma}^2, \tag{2.1}$$

where $\eta_0 = \eta_p + \eta_s$ is the total viscosity (with η_p and η_s the polymer and solvent viscosities, respectively), ζ is the ratio of solvent to total viscosities, $\dot{\gamma}$ is the shear rate and λ is the relaxation time. For the composition of the BF-I fluid, we found that $\zeta = 0.225$ and $\eta_0 = 0.844\,\text{Pa s}$, $\beta = 0.225$. By fitting (2.1) to the rheological data, we obtain the relaxation time of the Boger fluid, $\lambda = 0.51\,\text{s}$.

The steady and oscillatory shear tests of the BF-II fluid are shown in figure 2. The fluid showed a nearly constant viscosity for the entire range of shear rates. The viscosity and the shear stress of the Boger fluid were fit to a power-law model, leading to a power-law index $n = 0.98$. Therefore, we consider that the viscosity of the Boger fluid is effectively constant. The first normal stress difference (not shown) was not quadratic with shear rate.

To find the relaxation time for the BF-II fluid, we used the oscillatory tests. Since there is no crossover of the storage modulus, $G'(\omega)$, and loss modulus, $G''(\omega)$, for this fluid, as shown in figure 2(*b*), the generalized Maxwell model was used to fit the experimental values of $G'(\omega)$ and $G''(\omega)$ following Baumgaertel & Winter (1989), Liu, Powers & Breuer (2011), and Espinosa-Garcia, Lauga & Zenit (2013). The storage modulus and loss modulus are given by

$$G'(\omega) = \sum_{i=1}^{N} \frac{g_i\lambda_i^2\omega^2}{1 + \lambda_i^2\omega^2} \quad \text{and} \quad G''(\omega) = \omega\eta_s + \sum_{i=1}^{N} \frac{g_i\lambda_i\omega}{1 + \lambda_i^2\omega^2}, \tag{2.2a,b}$$

where ω is the oscillation frequency, η_s is the viscosity of the Newtonian solvent, and g_i is the corresponding fitting parameter for relaxation time τ_i. The corresponding relaxation time is determined by fitting the experimental data using (2.2a,b) with $N = 4$.

3. Results and discussion

3.1. *Experimental results*

Figure 3 shows the experimental results of the levitation height, h_L, as a function of rotational speed, Ω, for all the spheres tested in the Boger fluids. In the case of Newtonian fluids (data not shown), the levitation distance is zero for all spheres and rotational speeds.
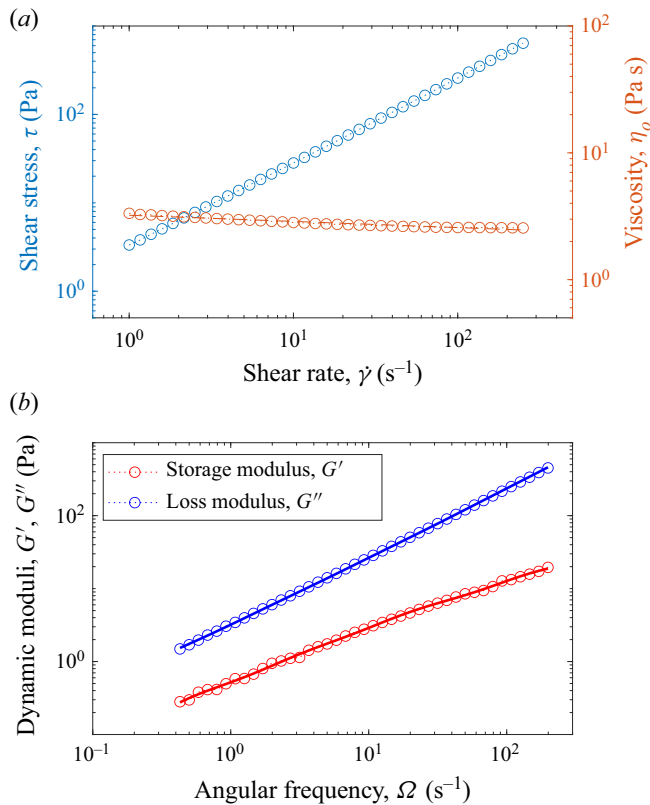
Y. Su, A. Castillo, O.S. Pak, L. Zhu and R. Zenit

Figure 2. Rheology of the BF-II fluid: (*a*) shear stress τ (left axis) and viscosity η_o (right axis) as a function of shear rate $\dot{\gamma}$; (*b*) oscillation test for the relaxation time measurement, storage modulus (red circles) and loss modulus (blue circles) versus oscillating frequency Ω. The solid lines show the fit to the data using the generalized Maxwell model (2.2*a,b*).

This is expected since there is no shear-induced normal stress generated for Newtonian fluids. When experiments were conducted with the spheres immersed in the Boger fluids (BF-I and BF-II), a significant levitation height h_L was observed, with the error bars showing the variations of the levitation motion in the equilibrium state (gravity force balanced by levitating force). Videos of associated experiments can be found in the supplementary materials https://doi.org/10.1017/jfm.2022.418. In general, the levitation height increases with the rotating speed Ω, indicating that there is a significant viscoelastic reaction from the fluid as a result of the rotation-induced shear in the gap between the sphere and the wall. Clearly, the levitation is a result of solely the viscoelastic nature of the fluid. The Reynolds number based on the rotating speed ranges from 0.5 to 3, for which inertial effects are small.

In particular, from the data shown in figure 3, we can see that for spheres of the same diameter (D2, black solid circle and D3, blue solid diamond), the levitation height is larger for the sphere of a smaller density (D2, black solid circle) at the same rotation rate; for spheres of the same density (D1, green solid square and D4, red solid reverse triangle), the levitation height is larger for the sphere of a larger diameter (D4, red solid reverse triangle) considering the same rotational speed. To understand the levitation height dependence on the experimental parameters (density and diameter), we compose a theoretical model that

943 A23-6
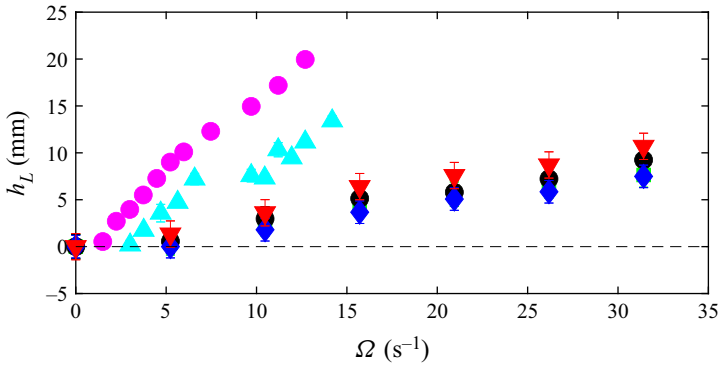
Figure 3. Levitation height h_L (mm) as a function of the rotational speed Ω (s^{-1}) for the Boger fluids (BF-I and BF-II). The symbols for the experiments correspond to those in table 1. The dashed line shows the measurements for the Newtonian case (no levitation observed).

can be compared with the experimental results. The model, however, is valid only for small values of the Deborah number *De*.

3.2. *Theoretical model*

We consider a sphere of diameter D rotating at a constant velocity Ω near an infinitely large wall (see figure 1a). The rotational axis is along the wall-normal direction (z), and the bottom of the sphere is above the wall by distance h. Hence the configuration is axisymmetric and can be described by the r, z cylindrical coordinates. The density of the sphere is assumed to be larger than that of the carrier fluid, hence their density difference satisfies $\Delta\rho > 0$. We use the the Oldroyd-B constitutive model to capture the viscoelasticity of the fluid, which was shown to agree well with the rheological behaviour of fluid BF-I. Although the Oldroyd-B model does not predict the second normal stress difference, the magnitude of the second normal stress difference is typically much smaller compared with that of the first normal stress difference, making the Oldroyd-B model a reasonable approximation of a Boger fluid. The governing equations of the fluid are

$$\left.\begin{aligned} \nabla \cdot \boldsymbol{u} = 0, \\ \nabla \cdot \boldsymbol{\sigma} = \boldsymbol{0}, \end{aligned}\right\} \tag{3.1}$$

where $\boldsymbol{\sigma} = -p\boldsymbol{I} + \eta_s\boldsymbol{E} + \boldsymbol{\tau}_p$, p and $\boldsymbol{u}$ denote the pressure and velocity, respectively, and $\boldsymbol{E} = \nabla\boldsymbol{u} + (\nabla\boldsymbol{u})^{\mathrm{T}}$ denotes the rate of strain tensor. The relative viscosity $\zeta = \eta_s/\eta_0 < 1$ is defined as the ratio between η_s and the total viscosity η_0. The polymeric stress $\boldsymbol{\tau}_p$ is governed by the upper-convected Maxwell equation

$$\lambda\overset{\triangledown}{\boldsymbol{\tau}}_p + \boldsymbol{\tau}_p = \eta_p\boldsymbol{E}, \tag{3.2}$$

where the upper-convected derivative $\overset{\triangledown}{A}$ on a tensor A is defined as $\overset{\triangledown}{A} = \partial A/\partial t + \boldsymbol{u} \cdot \nabla A - (\nabla\boldsymbol{u})^{\mathrm{T}} \cdot A - A \cdot \nabla\boldsymbol{u}$. Here, λ denotes the relaxation time of the polymeric fluid, and the polymeric viscosity is $\eta_p = (1 - \zeta)\eta_0$.

Due to axisymmetry, the levitating force due to the viscoelastic stress $\boldsymbol{F}_H$ is along the z direction, which should balance the gravity-induced force $\boldsymbol{F}_G = -(\pi/6)\,\Delta\rho\,gD^3\,\boldsymbol{e}_z$, where g denotes the gravitational acceleration. For a given polymeric fluid and a given rotational

speed, we seek a levitation height h_L such that $\boldsymbol{F}_H(\Omega, h = h_L) = -\boldsymbol{F}_G$, when the rotating sphere suspends above the wall by a finite distance, with $h_L > 0$.

3.2.1. *Non-dimensionalization*

We scale lengths by D, time by $1/\Omega$, velocities by ΩD, and stresses by $\eta_0 \Omega$, with the non-dimensional variables denoted with tildes. The non-dimensional governing equations are therefore given by

$$\left.\begin{aligned} \tilde{\boldsymbol{\nabla}} \cdot \tilde{\boldsymbol{u}} &= 0, \\ -\tilde{\boldsymbol{\nabla}}\tilde{p} + \zeta \, \nabla^2 \tilde{\boldsymbol{u}} + \tilde{\boldsymbol{\nabla}} \cdot \tilde{\boldsymbol{\tau}}_p &= \boldsymbol{0}, \\ De \, \tilde{\boldsymbol{\tau}}_p + \overset{\triangledown}{\tilde{\boldsymbol{\tau}}}_p &= (1 - \zeta)\tilde{\boldsymbol{E}}, \end{aligned}\right\} \tag{3.3}$$

where $De = \lambda\Omega$ is the Deborah number indicating the non-dimensional relaxation time of the viscoelastic fluid. We hence seek a non-dimensional levitation height $\tilde{h} = \tilde{h}_L$ such that

$$\tilde{F}_H(De, \tilde{h}_L) = G, \tag{3.4}$$

where

$$G = \frac{\pi g D \, \Delta\rho}{6\eta_0 \Omega} \tag{3.5}$$

is the dimensionless gravitational force.

3.2.2. *Small Deborah number analysis: a reciprocal theorem approach*

We first consider the small-De limit of (3.3) and adopt the second-order fluid model to describe the first departure from Newtonian behaviour. In a retarded motion expansion, the non-dimensional shear stress tensor of a second-order fluid reads

$$\tilde{\boldsymbol{\tau}} = \tilde{\boldsymbol{E}} - De_0 \left(\overset{\triangledown}{\tilde{\boldsymbol{E}}} - \frac{2\Psi_2}{\Psi_1} \, \tilde{\boldsymbol{E}} \cdot \tilde{\boldsymbol{E}} \right), \tag{3.6}$$

where Ψ_1 and Ψ_2 are the first and second normal stress coefficients, respectively. Here, $De_0 = \Psi_1 \Omega / \eta$ defines the Deborah number of the second-order fluid, and it relates to De by $De_0 = (1 - \zeta)De$. For comparison with the Oldroyd-B model, where the second normal stress difference is zero, we set $\Psi_2 = 0$ to recover the Oldroyd-B model in the small-De limit.

First, we calculate asymptotically the hydrodynamic force $\tilde{\boldsymbol{F}}_H = \tilde{F}_H \boldsymbol{e}_z$ on a rotating sphere suspended at a given height $\tilde{h}$. We expand the variables in powers of De_0 as

$$\{\tilde{\boldsymbol{\sigma}}, \tilde{\boldsymbol{u}}, \tilde{\boldsymbol{E}}, \tilde{\boldsymbol{F}}_H\} = \{\tilde{\boldsymbol{\sigma}}_0, \tilde{\boldsymbol{u}}_0, \tilde{\boldsymbol{E}}_0, \tilde{\boldsymbol{F}}_0\} + De_0\{\tilde{\boldsymbol{\sigma}}_1, \tilde{\boldsymbol{u}}_1, \tilde{\boldsymbol{E}}_1, \tilde{\boldsymbol{F}}_1\} + O(De_{so}^2). \tag{3.7}$$

The zeroth-order solution $\{\tilde{\boldsymbol{u}}_0, \tilde{\boldsymbol{\sigma}}_0 = -\tilde{p}_0\boldsymbol{I} + \tilde{\boldsymbol{E}}_0\}$ is a known Newtonian (Stokes flow) solution for a rotating sphere above a wall (Jeffery 1915), where the zeroth-order hydrodynamic force on the sphere is $\tilde{\boldsymbol{F}}_0 = \boldsymbol{0}$. Levitation of a rotating sphere near a wall is therefore impossible in a Newtonian fluid.

Next, we calculate the first-order non-Newtonian correction $\{\tilde{\boldsymbol{u}}_1, \tilde{\boldsymbol{\sigma}}_1 = -\tilde{p}_1\boldsymbol{I} + \tilde{\boldsymbol{E}}_1 - \overset{\triangledown}{\tilde{\boldsymbol{E}}}_0\}$ via a reciprocal theorem approach (Lauga 2014; Elfring 2017; Masoud & Stone 2019). By considering an auxiliary problem in Stokes flow $(\tilde{\boldsymbol{u}}', \tilde{\boldsymbol{\sigma}}')$, where a sphere translates
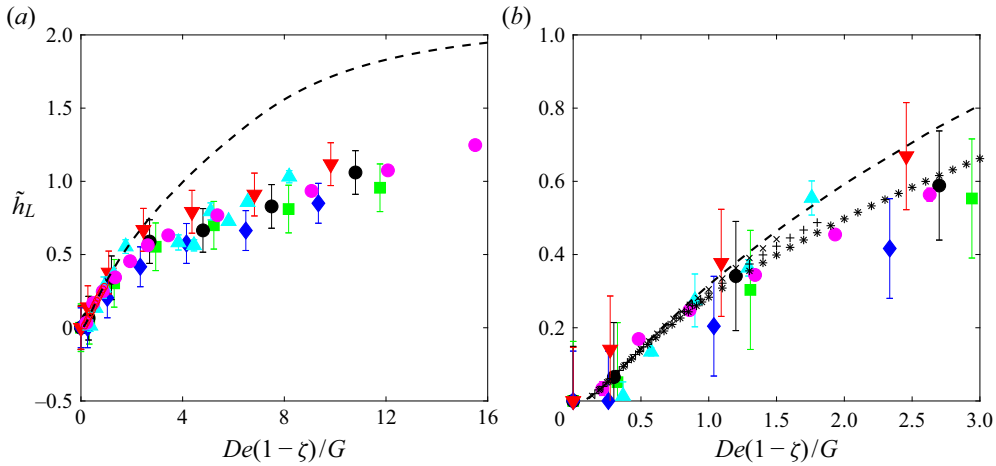
(*a*)

(*b*)

Figure 5. (*a*) Dimensionless levitation height $\tilde{h}_L = h_L/D$ of the rotating sphere as a function of the dimensionless group $De\,(1-\zeta)/G$. The dashed line represents predictions by the asymptotic theory in the small-*De* limit, whereas the symbols correspond to experimental data presented previously. (*b*) A magnified view of results in (*a*) for small values of $De\,(1-\zeta)/G$, with the addition of results from numerical simulations for $De = 1$ (×), $De = 1.5$ (+), and $De = 2$ (∗). In all simulations, $\zeta = 0.225$.

small; in this regime, the data collapse well, confirming that the levitation height depends only on the dimensionless group $De\,(1-\zeta)/G$.

4. Conclusions

In this study, we conducted experiments and theoretical analysis on spheres of different sizes and densities immersed in two fluids: Newtonian and viscoelastic Boger fluids. With a constant rotating rate, the sphere levitates to a fixed distance from the bottom in the viscoelastic fluid, instead of no levitation in Newtonian fluids. The viscoelastic normal stress between the sphere and the bottom wall is responsible for this 'viscoelastic levitation'. In the small-*De* asymptotic analysis, based on the balance between the viscoelastic levitating force and the gravitational force on the sphere, a dimensionless group was formulated in terms of the Deborah number *De*, the relative viscosity ζ, and the dimensionless gravitational force *G*. Using this dimensionless group, experimental measurements of the levitation height display a good collapse onto a single curve. The agreement between experiments and asymptotic results is very good when *De* is small, consistent with the small-*De* assumption in the asymptotic analysis.

It can be argued that this configuration can be used as a rheometer. If the density and size of a sphere that rotates above a wall are known, then a measurement of the levitation height can be used to infer the value of the Deborah number, from which the fluid relaxation time could be obtained. This method could be implemented easily considering the experimental device shown here, for small Deborah numbers. Other rotation directions and non-constant rotation speeds could also be considered to obtain other viscoelastic characteristics of the fluid. We plan to pursue these ideas in the future.

Author ORCIDs.

Yunxing Su https://orcid.org/0000-0001-5981-1228;

On Shun Pak https://orcid.org/0000-0003-1510-7049;

Lailai Zhu https://orcid.org/0000-0002-3443-0709;

Roberto Zenit https://orcid.org/0000-0002-2717-4954.

REFERENCES

ANGELES, V., GODÍNEZ, F.A., PUENTE-VELAZQUEZ, J.A., MENDEZ-ROJANO, R., LAUGA, E. & ZENIT, R. 2021 Front–back asymmetry controls the impact of viscoelasticity on helical swimming. *Phys. Rev. Fluids* **6**, 043102.

D'AVINO, G., MAFFETTONE, P.L., GRECO, F. & HULSEN, M.A. 2010 Viscoelasticity-induced migration of a rigid sphere in confined shear flow. *J. Non-Newtonian Fluid Mech.* **165** (9–10), 466–474.

BAUMGAERTEL, M. & WINTER, H.H. 1989 Determination of discrete relaxation and retardation time spectra from dynamic mechanical data. *Rheol. Acta* **28**, 511–519.

BINAGIA, J.P. & SHAQFEH, E.S.G. 2021 Self-propulsion of a freely suspended swimmer by a swirling tail in a viscoelastic fluid. *Phys. Rev. Fluids*. **6** (5), 053301.

BOGER, D.V. 1977 A highly elastic constant-viscosity fluid. *J. Non-Newtonian Fluid Mech.* **3**, 87–91.

BRENNER, H. 1961 The slow motion of a sphere through a viscous fluid towards a plane surface. *Chem. Engng Sci.* **16** (3–4), 242–251.

CASTILLO, A., MURCH, W.L., EINARSSON, J., MENA, B., SHAQFEH, E.S.G. & ZENIT, R. 2019 Drag coefficient for a sedimenting and rotating sphere in a viscoelastic fluid. *Phys. Rev. Fluids* **4**, 063302.

DADDI-MOUSSA-IDER, A., LISICKI, M., HOELL, C. & LOWEN, H. 2018 Swimming trajectories of a three-sphere microswimmer near a wall. *J. Chem. Phys.* **148**, 134904.

DATT, C., ZHU, L., ELFRING, G.J. & PAK, O.S. 2015 Squirming through shear-thinning fluids. *J. Fluid Mech.* **784**, R1.

DUNN, P.F. & PICOLOGLOU, B.F. 1976 Viscoelastic properties of cumulus oophorus. *Biorheology* **13**, 379–384.

ELFRING, G.J. 2017 Force moments of an active particle in a complex fluid. *J. Fluid Mech.* **829**, R3.

ESPINOSA-GARCIA, J., LAUGA, E. & ZENIT, R. 2013 Fluid elasticity increases the locomotion of flexible swimmers. *Phys. Fluids* **25** (3), 031701.

GODÍNEZ, F.A., CHÁVEZ, O. & ZENIT, R. 2012 Note: design of a novel rotating magnetic field device. *Rev. Sci. Instrum.* **83**, 066109.

HALOW, J.S. & WILLS, G.B. 1970 Experimental observations of sphere migration in Couette systems. *Ind. Engng Chem. Fundam.* **9** (4), 603–607.

HO, B.P. & LEAL, L.G. 1976 Migration of rigid spheres in a two-dimensional unidirectional shear flow of a second-order fluid. *J. Fluid Mech.* **76** (4), 783–799.

JAMES, D. 2009 Boger fluids. *Annu. Rev. Fluid Mech.* **41**, 129–142.

JEFFERY, G.B. 1915 On the steady rotation of a solid of revolution in a viscous fluid. *Proc. Lond. Math. Soc.* **2** (1), 327–338.

KATZ, D.F., MILLS, R.N. & PRITCHETT, T.R. 1978 The movement of human spermatozoa in cervical mucus. *J. Reprod. Fertil.* **53**, 259–265.

KEIM, N.C., GARCIA, M. & ARRATIA, P.E. 2012 Fluid elasticity can enable propulsion at low Reynolds number. *Phys. Fluids* **24**, 081703.

KEUNINGS, R. 1986 On the high Weissenberg number problem. *J. Non-Newtonian Fluid Mech.* **30**, 209–226.

LARSON, R.G. 1999 *The Structure and Rheology of Complex Fluids*. Oxford University Press.

LAUGA, E. 2014 Locomotion in complex fluids: integral theorems. *Phys. Fluids* **26** (8), 081902.

LAUGA, E. & POWERS, T.R. 2009 The hydrodynamics of swimming microorganisms. *Rep. Prog. Phys.* **72**, 096601.

LI, G.-J. & ARDEKANI, A.M. 2014 Hydrodynamic interaction of microswimmers near a wall. *Phys. Rev.* E **90**, 013010.

LIU, B., POWERS, T.R. & BREUER, K.S. 2011 Force-free swimming of a model helical flagellum in viscoelastic fluids. *Proc. Natl Acad. Sci. USA* **108** (49), 19516–19520.

MASOUD, H. & STONE, H.A. 2019 The reciprocal theorem in fluid dynamics and transport phenomena. *J. Fluid Mech.* **879**, P1.

MOROZOV, A. & SPAGNOLIE, S.E. 2015 Introduction to complex fluids. In *Complex Fluids in Biological Systems. Experiment, Theory, and Computation* (ed. S.E. Spagnolie), chap. 1, pp. 3–52. Springer.

NADAL, F., PAK, O.S., ZHU, L., BRANDT, L. & LAUGA, E. 2014 Rotational propulsion enabled by inertia. *Eur. Phys. J.* E **37** (7), 60.

NORMAND, T. & LAUGA, E. 2008 Flapping motion and force generation in a viscoelastic fluid. *Phys. Rev* E **78**, 061907.

OLDROYD, J.G. 1950 On the formulation of rheological equations of state. *Proc. R. Soc.* **200**, 523–541.

OWENS, R.G. & PHILLIPS, T.N. 2002 *Computational Rheology*, vol. 14. World Scientific.

PAK, O.S., NORMAND, T. & LAUGA, E. 2010 Pumping by flapping in a viscoelastic fluid. *Phys. Rev.* E **81**, 036312.

PAK, O.S., ZHU, L., BRANDT, L. & LAUGA, E. 2012 Micropropulsion and microrheology in complex fluids via symmetry breaking. *Phys. Rev. Fluids* **24**, 103102.

PUENTE-VELÁZQUEZ, J.A., GODÍNEZ, F.A., LAUGA, E. & ZENIT, R. 2019 Viscoelastic propulsion of a rotating dumbbell. *Microfluid Nanofluid* **23**, 108.

PURCELL, E.M. 1977 Life at low Reynolds number. *Am. J. Phys.* **45**, 3–11.

SUAREZ, S.S. & PACEY, A.A. 2006 Sperm transport in the female reproductive tract. *Hum. Reprod. Update* **1**, 23–37.

WIOLAND, H., WOODHOUSE, F.G., DUNKEL, J. & GOLDSTEIN, R.E. 2016 Ferromagnetic and antiferromagnetic order in bacterial vortex lattices. *Nat. Phys.* **12**, 341–345.

WIOLAND, H., WOODHOUSE, F.G., DUNKEL, J., KESSLER, J.O. & GOLDSTEIN, R.E. 2013 Confinement stabilizes a bacterial suspension into a spiral vortex. *Phys. Rev. Lett.* **110**, 268102.

WOODHOUSE, F.G. & DUNKEL, J. 2017 Active matter logic for autonomous microfluidics. *Nat. Commun.* **8**, 15169.

WOODHOUSE, F.G. & GOLDSTEIN, R.E. 2012 Spontaneous circulation of confined active suspensions. *Phys. Rev. Lett.* **109**, 168105.

ZHU, L., LAUGA, E. & BRANDT, L. 2012 Self-propulsion in viscoelastic fluids: pushers vs pullers. *Phys. Fluids* **24**, 051902.